Int. J. Electrochem. Sci., 13 **(2018)** 7397 – 7407, doi: 10.20964/2018.08.20

International Journal of
ELECTROCHEMICAL
SCIENCE
www.electrochemsci.org

Hybrid MnO/Ni Li-ion Battery Anode Material with Enhanced Capacity Retention

Muharrem Kunduraci

Department of Mechanical Engineering, Faculty of Engineering, University of Turkish Aeronautical Association, Ankara 06790, Turkey
E-mail: kunduraci.m@hotmail.com

Received: 1 April 2018 / *Accepted:* 22 May 2018 / *Published:* 5 July 2018

Intimately mixed MnO/Ni hybrid materials are synthesized using a two-step process; Pechini process followed by a high temperature reduction step. As-prepared materials were characterized by X-ray diffraction, transmission electron microscopy and electrochemical tests. $(MnO)_{1-x}/(Ni)_x$ hybrid materials with x=0, 0.2 and 0.5 mole ratios are electrochemically evaluated as anode materials for lithium-ion batteries. The battery tests conclusively show that the coulombic efficiency, capacity utilization factor, percentage capacity retention and high rate performance values of control MnO material are enhanced with the presence of nearby metallic Ni nanoparticles. Oxide/metal hybrid material could be a cheaper alternative to commonly known oxide/graphene system.

Keywords: lithium-ion battery; conversion anode, oxide/metal hybrid

1. INTRODUCTION

Hybrid materials are interesting and technologically very significant group of materials. They find widespread use in fields such as electrochemical storage and conversion [1-9], mechanical [10-11], optical [12], thermal [13] applications. In electrochemical applications such batteries and fuel cells, hybrid materials are composed of one electronically conducting and one ionically conducting (typically Li^+, H^+ or O^{2-}) component. While the ionic component is directly involved in electrochemical activity or reactions, the electronic component simply helps with the electron transport. The synergy formed between these two materials enables improved electrochemical performance.

The surface of anode materials are covered with insulating SEI (solid electrolyte interface) layer during cycling and its surface electronic conductivity degrades over time. Also, up to 200% increase in anode volume during lithiation exacerbates this situation as more anode surface is exposed

to the electrolyte. The coating or wrapping of battery anode materials with graphene has been demonstrated as an effective approach to mitigate this problem [14-16]. Graphene has been popularized due to its low weight and high electronic conductivity. However, its synthesis as well as the process of bringing it together with electroactive material to form a homogeneous bi-component structure can involve many steps, thereby making it too expensive and tedious.

On the other hand, hybrid oxide/metal system can be easily synthesized in a more cost-effective and simplier way. Some examples include electroplating [17], electrostatic spray deposition [18] and dealloying [19]. Among the transition metal oxide anodes, manganese based materials have attracted lots of interest due to their low cost and high specific capacities [20-22]. In this work, nanostructured $(MnO)_{1-x}/(Ni)_x$ hybrid materials with varying x values are synthesized by wet chemistry followed by a quick thermal reduction step and electrochemically evaluated for their lithium storage capacities. The hybrid materials are shown to exhibit better electrochemical performances over control MnO anode material.

2. EXPERIMENTAL

2.1. Material Synthesis

$(MnO)_{1-x}/(Ni)_x$ hybrid materials where x=0, 0.2 and 0.5 in moles [i.e. MnO, $(MnO)_{0.8}/(Ni)_{0.2}$ and $MnO)_{0.5}/(Ni)_{0.5}$] were prepared by a two-step process. Schematic of the synthesis process is provided in Figure S1. In the first step, oxide precursors were prepared by Pechini process [23]. Citric acid was dissolved in ethylene glycol at 120 °C on hot plate with a mole ratio of 1-to-4. Separately, an aqueous solution of metal nitrate salts were prepared using deionized water and added drop-by-drop to the first solution. At this temperature, chelation of metal ions and organic acid took place. At the end of this step, the dark colored solution was heated to 160 °C for esterification. The solution turned into a dark and solid residue with evaporation of water and excess ethylene glycol. The solid material was ground and heated to 500 °C for 1 hr in air. Crystalline oxide precursor with no residual organics was obtained. In the second step, precursor oxide material was heated to 700 °C under flowing H_2/Argon mixture for 1 hr to get MnO or $(MnO)_{1-x}/(Ni)_x$ hybrid materials.

2.2. Materials Characterization

The morphological properties of the as-prepared anode materials were investigated using transmission electron microscope (TEM; FEI-Tecnai G2 F30) at 200 kV. Samples were dispersed in ethanol and loaded onto a holey carbon coated copper grid. Besides imaging, mapping of Mn and Ni elements over selected areas was also carried out. Crystal phase analysis of oxide material was realized by powder X-ray diffraction using Panalytical X'pert Multi-Purpose. The patterns were attained in the range of 2θ = 15–75° using Bragg–Brentano geometry (Cu Kα radiation, $\boldsymbol{\lambda}$= 0.15418 nm).

2.3. Electrochemical Characterization

In order to prepare the anode slurries, PVDF binder was first dissolved in N-methyl-2-pyrrolidone solvent. Later, anode material and conductive carbon Super P were added to this solution and mixed for 1 hr at 800 rpm. The slurry was cast and the solvent was removed by vacuum drying the electrode at 70 °C overnight. It was then quickly transferred into argon filled glovebox (O_2 < 0.5 ppm, H_2O < 0.5 ppm). The electrode consisted of 60 wt% of anode material, 15 wt% of conductive carbon and 25 wt% of PVDF binder. Half cells [$(MnO)_{1-x}/(Ni)_x$ vs. Li metal] were built using custom-made cells. Celgard and glass microfiber filter separators were used. The electrolyte was 1 M LiTFSI dissolved in EC:DMC (1:1) solution. After sealing, the cells were rested for 8 hr prior to testing. Battery cycle life tests were executed using Landt CT2001 multichannel potentiostat/galvanostat between 0.01 V and 3 V potential window at a current density of 100 mA g^{-1}. AC impedance spectroscopy analyses were conducted using the same unit by applying 5 mV alternating voltage.

3. RESULTS AND DISCUSSION

The phase analyses of anode materials were carried out using X-ray diffraction and their patterns are given in Figure 1.

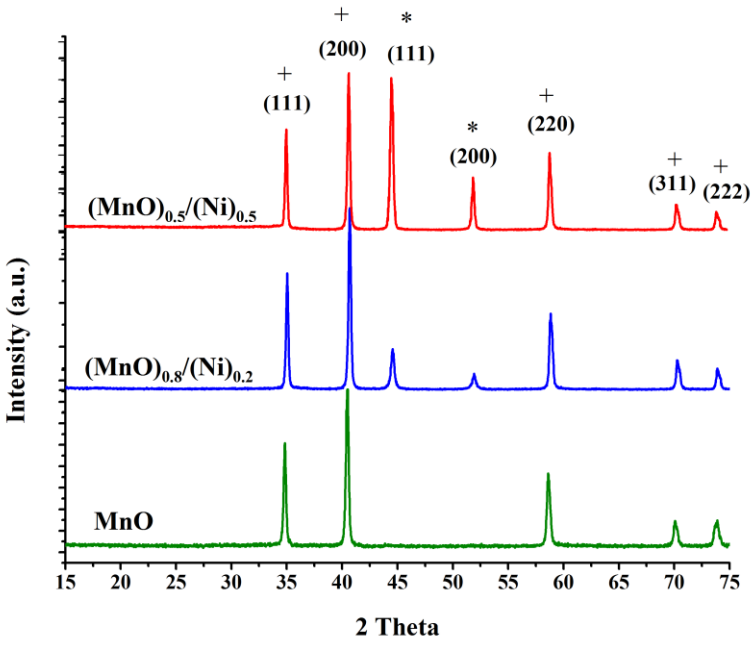

Figure 1. X-ray diffraction patterns of $(MnO)_{1-x}/(Ni)_x$ hybrid materials where x=0, 0.2 or 0.5. Reflection peaks belonging to MnO and Ni phases are marked with + and * signs, respectively.

The spectrum of baseline MnO (JCPDS No: *07-0230*) consists of 5 peaks all belonging to this phase with no sign of any secondary impurity phase. The diffraction peaks are at 2θ angle around 35, 41, 59, 70 and 74° indexed to (111), (200), (220), (311) and (222) reflections. In hybrid materials, two extra

peaks appear. These peaks are located at 2θ angle around 44.5 and 52° and belong to (111) and (200) reflection of fcc Ni metal (JCPDS No: 04-0850). Nickel peaks are more intense in $(MnO)_{0.5}/(Ni)_{0.5}$ due to the larger amount of metallic nickel.

Transmission electron microscope (TEM) was utilized to investigate the morphological characteristics of $(MnO)_{1-x}/(Ni)_x$ hybrid materials. TEM images of MnO (x=0) and $(MnO)_{0.5}/(Ni)_{0.5}$ materials are provided in Figure 2.a-b.

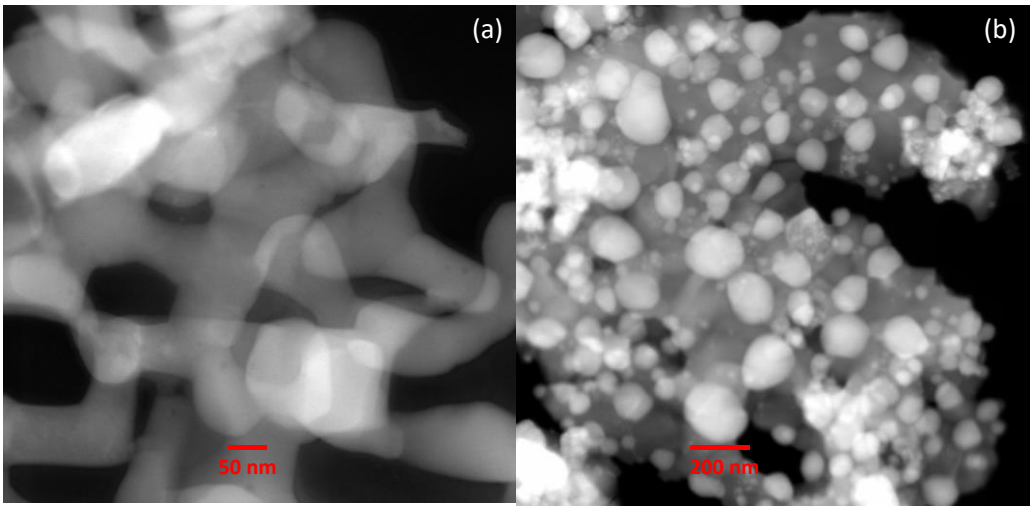

Figure 2. Transmission electron microscope images of a) MnO and b) $(MnO)_{0.5}/(Ni)_{0.5}$ anode materials. The bars are in 50 nm and 200 nm in length, respectively.

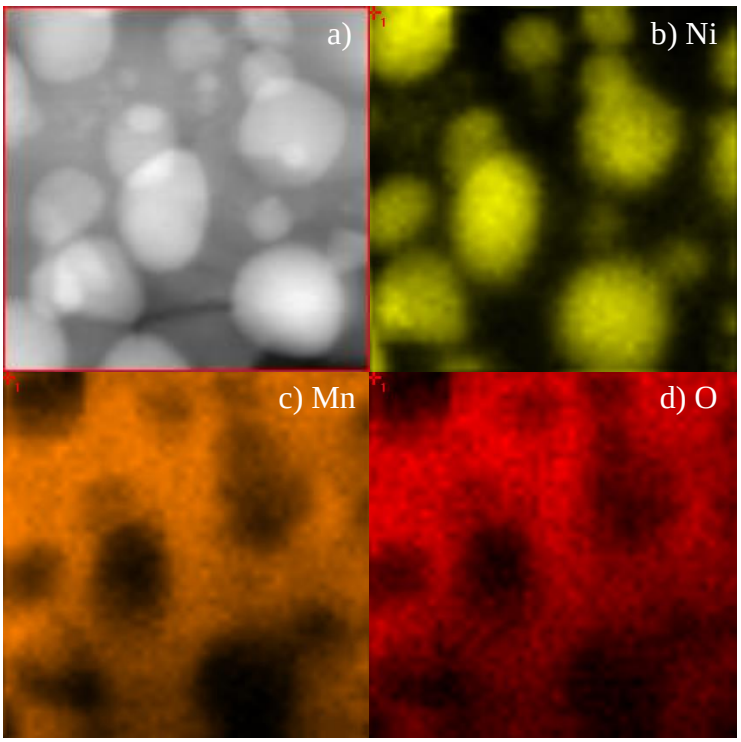

Figure 3. a) Transmission electron microscope image of $(MnO)_{0.5}/(Ni)_{0.5}$ hybrid material. Elemental mapping results taken from the same region b) Ni-K orbital b) Mn-K orbital d) O-K orbital

MnO material is made of interconnected particles that are 100 nm in diameter. This nanostructured morphology will be conducive to lithium-ion transport during cell charge and discharge. In case of hybrid $(MnO)_{0.5}/(Ni)_{0.5}$, an unique and interesting morphology is observed. The material consists of a dark-colored background and bright-colored individual and spherical-shaped particles. These particles are around 100-150 nm in diameter and uniformly distributed, thereby providing excellent coverage. In order to differentiate these two distinct materials, elemental mapping analysis was performed over a region given in Figure 3.a. The individual distribution of Mn, Ni and O elements are illustrated in Figure 3.b-d. It can be concluded without doubt that the shiny regions belong to nickel metal while darker regions are made of MnO phase. Such intimate and homogeneous mixing of oxide and metal particles looks promising to have good electrochemical activity. Besides elemental mapping over an area, point elemental analysis was also carried out on bright and dark regions separately. The results are given in Figure S2 and in agreement with mapping results.

The source of electrochemical activity in anode materials is based on the reaction in equation 1 [24-25];

$$MnO + 2Li^+ + 2e^- \leftrightarrow Mn + Li_2O \qquad (1)$$

In hybrid materials, nickel atoms were assumed to be electrochemically inactive and only contribute to the electron transport on the surface of MnO particles. Based on this assumption, the theoretical lithium-ion capacities of MnO, $(MnO)_{0.8}/(Ni)_{0.2}$ and $(MnO)_{0.5}/(Ni)_{0.5}$ anode materials are calculated to be 755, 626 and 413 mAh g^{-1}, respectively.

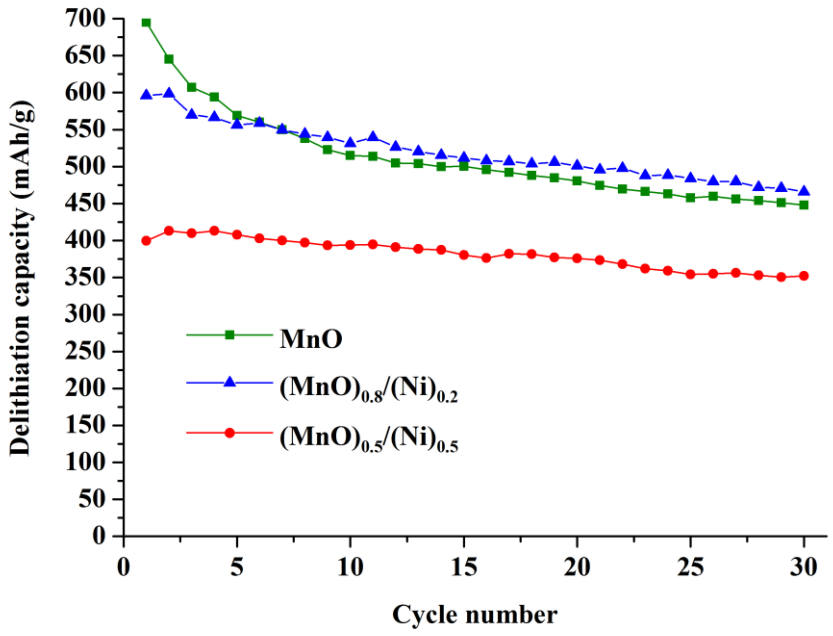

Figure 4. Variation of charge (delithiation) capacity of $(MnO)_{1-x}/(Ni)_x$ hybrid anode materials with cycle number

The charge (delithiation) capacities of anode materials are plotted in Figure 4 as a function of cycle number. The cells were charged and discharged at 100 mA g^{-1} current density. Baseline MnO

anode material has a first cycle discharge (lithiation) capacity of 951 mAh g^{-1} and charge capacity of 695 mAh g^{-1}, corresponding to 73% coulombic efficiency. The charge capacities are in line with previous literature data (Table S1). The capacity utilization factor, which is defined here as the ratio of actual to theoretical charge capacities, is calculated to be 92.0% for the same material. As for $(MnO)_{0.8}/(Ni)_{0.2}$ and $(MnO)_{0.5}/(Ni)_{0.5}$ anode materials, these values were calculated to be 75% and 75.5% for coulombic efficiencies and 95.2% and 96.8% for capacity utilization factor, respectively. It appears that nanosized metallic nickel particles are conducive to the reversibility of conversion reaction.

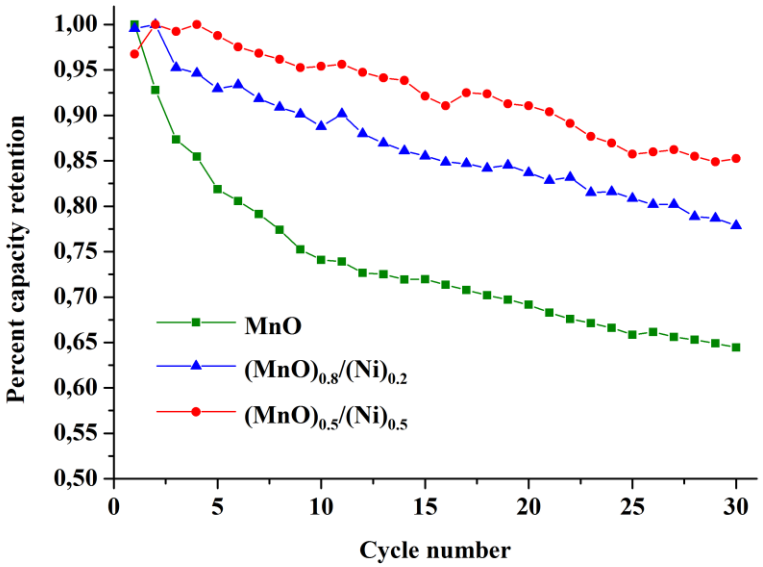

Figure 5. Percentage capacity retention of $(MnO)_{1-x}/(Ni)_x$ hybrid anode materials as a function of cycle number. The retention values were normalized with respect to the highest capacity.

The charge capacities of anode materials in the successive cycles were normalized with respect to the first cycle and are plotted as a function of cycle number in Figure 5. The average capacity fading rate of nickel-free MnO material within these 30-cycle period is found to be 1.18% per cycle while it is 0.73% and 0.49% per cycle for $(MnO)_{0.8}/(Ni)_{0.2}$ and $(MnO)_{0.5}/(Ni)_{0.5}$ anode materials, respectively. The fast capacity decay observed in bare MnO anodes were attributed to the isolation and cracking of oxide particles [26]. The slower fading rates observed in hybrid materials demonstrate that metallic nickel particles help maintain electrical contact during large volume changes, thereby resulting in better preservation of electrochemical activity.

Previous studies demonstrated clearly that coating of oxide materials with conductive film help extract more capacities at higher current densities thanks to improved electron transport characteristics of anode material [27-28]. The sister cells of MnO and $(MnO)_{0.5}/(Ni)_{0.5}$ anode materials were prepared and charged at varying *C* rates in order to determine if nickel particles were also beneficial to high rate performance. The charge capacities of both anode materials obtained at different charging rates are given in Figure 6. The discharge (lithiation) rate was kept constant at 0.2*C*. The ratio of 3C-to-0.2C capacities were 0.72 for hybrid material and 0.45 for MnO only anode material. This results confirm the positive impact of metallic nickel nanoparticles at high current rates.

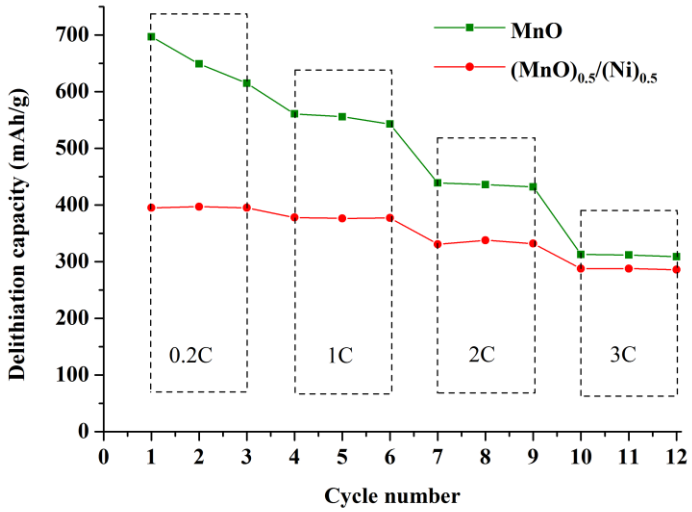

Figure 6. Delithiation (charge) capacities of MnO and $(MnO)_{0.5}/(Ni)_{0.5}$ anode materials at different *C* rates

In order to ensure that the better electrochemical performance observed in hybrid materials over baseline MnO material should be attributed solely to the presence of metallic nickel particles, charge and discharge voltage profiles were investigated. Such analysis was two-folded. In the first part, it was checked if the addition of nickel atoms changed the mechanisms of lithiation and delithiation processes. For this purpose, the voltage curves of MnO and $(MnO)_{0.5}/(Ni)_{0.5}$ anode materials are presented and compared in Figure 7.a-b.

Both profiles are consistent with previous studies [29-30]. Specifically, they are composed of a 0.2 V plateau in the first cycle which moves up to 0.6 V in the following cycles and a 1.2 V charge plateau. The discharge plateau is due to the reduction of Mn^{2+} ions to metallic state Mn^0 as given in equation 1 and the charge plateau corresponds to the reverse oxidation reaction. The strong resemblance of profiles indicates that metallic nickel particles do not interfere with (de)lithiation reactions. In the second part, the average charge and discharge potentials were calculated for different cycles and their differences were compared for MnO and $(MnO)_{0.5}/(Ni)_{0.5}$ anode materials in Figure 7.c. It is known that as battery materials degrade over several cycles, the voltage hysteresis or polarization enlarges due to the build-up of resistive layers on the surface of active material. The results show that the polarization is smaller for hybrid material during extended cycling, thereby proving that metallic nickel nanoparticles help maintain the surface electronic conductivity of MnO anode material.

Another manifestation of higher surface electronic conductivity on anode surface could be lower charge transfer resistance (R_{ct}). Tang *et. al*. synthesized 3D Cu/Fe_3O_4 anode and showed that hybrid material had lower R_{ct} than bare Fe_3O_4 film [2]. In order to reproduce this result, AC impedance analyses of cells made of MnO and $(MnO)_{0.5}/(Ni)_{0.5}$ anode materials were done. The Z-plots of cells are given in Figure 8. The profiles consist of a high frequency resistance, a middle frequency arc and a low frequency sloping line. The high frequency resistance corresponds to lithium-ion transport in electrolyte and is similar for both cells. The most obvious difference between two cells is based on the

charge transfer resistance obtained from middle frequency arc. This resistance is 56 Ω for MnO and 31 Ω for $(MnO)_{0.5}/(Ni)_{0.5}$ hybrid material. The significantly smaller R_{ct} for hybrid material strengthens the notion that the oxide/metal hybrid structure has improved electron transport characteristics than oxide only anode material.

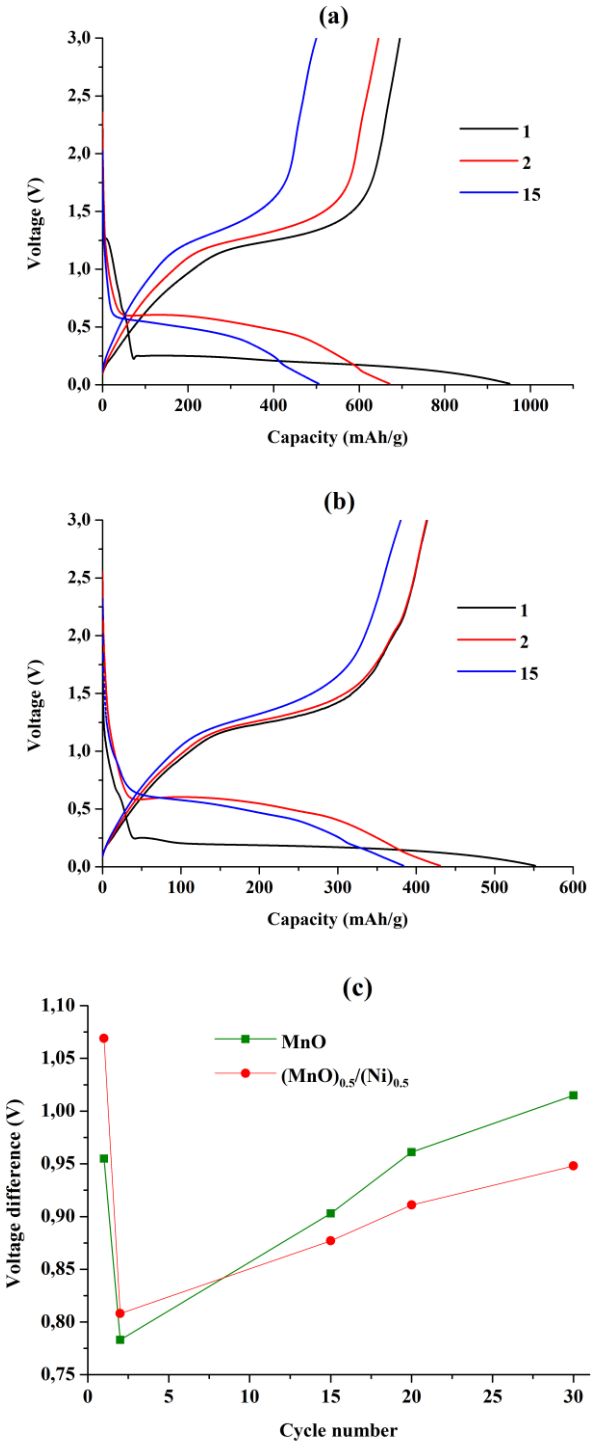

Figure 7. Charge and discharge voltage curves of a) MnO and b) $(MnO)_{0.5}/(Ni)_{0.5}$ anode materials at 1st, 2nd and 15th cycles. c) the difference in average charge and discharge voltages at different cycles for the same two anode materials.

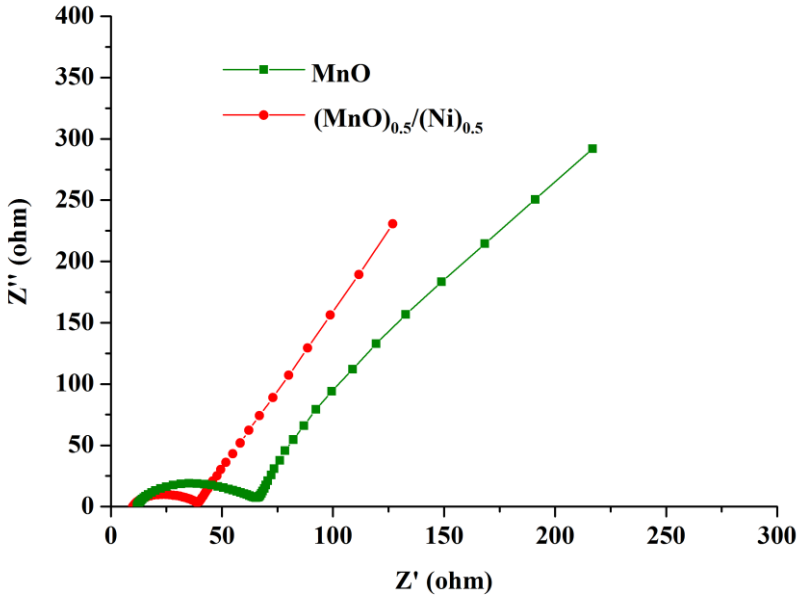

Figure 8. Z-plots of MnO and $(MnO)_{0.5}/(Ni)_{0.5}$ anode materials at the end of 1st charging step.

4. CONCLUSION

Nanostructured MnO, $(MnO)_{0.8}/(Ni)_{0.2}$ and $(MnO)_{0.5}/(Ni)_{0.5}$ hybrid materials were synthesized by wet chemistry step followed by a high temperature reduction step using H_2 gas. They were evaluated as lithium-ion battery anode materials and the electrochemical impact of metallic nickel nanoparticles were sought. Intimately mixed nature of MnO and Ni nanoparticles were found to be helpful to the capacity utilization factor, capacity retention and rate performance of active MnO component. Specifically, hybrid materials had longer cycle life as well as larger capacities at higher current densities. Also, the rate of polarization increase and impedance rise with cycling were lower for hybrid materials. On the other hand, nickel atoms are not directly involved in electrochemical activity, thereby causing reduction in theoretical specific gravimetric capacity. Although the use of electrochemically inactive nickel material in the range of 20-50 mole percentage is too much to be practical, it is believed that its use might be lowered to reasonable values (5-10 mole%) by optimizing their size, shape and distribution.

SUPPORTING INFORMATION

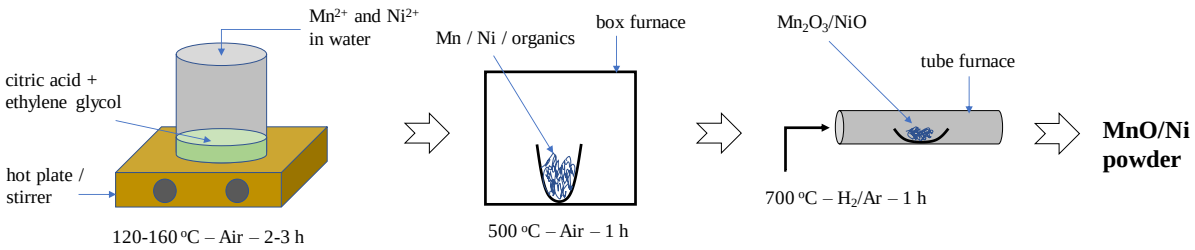

Figure S1. Schematic of synthesis procedure

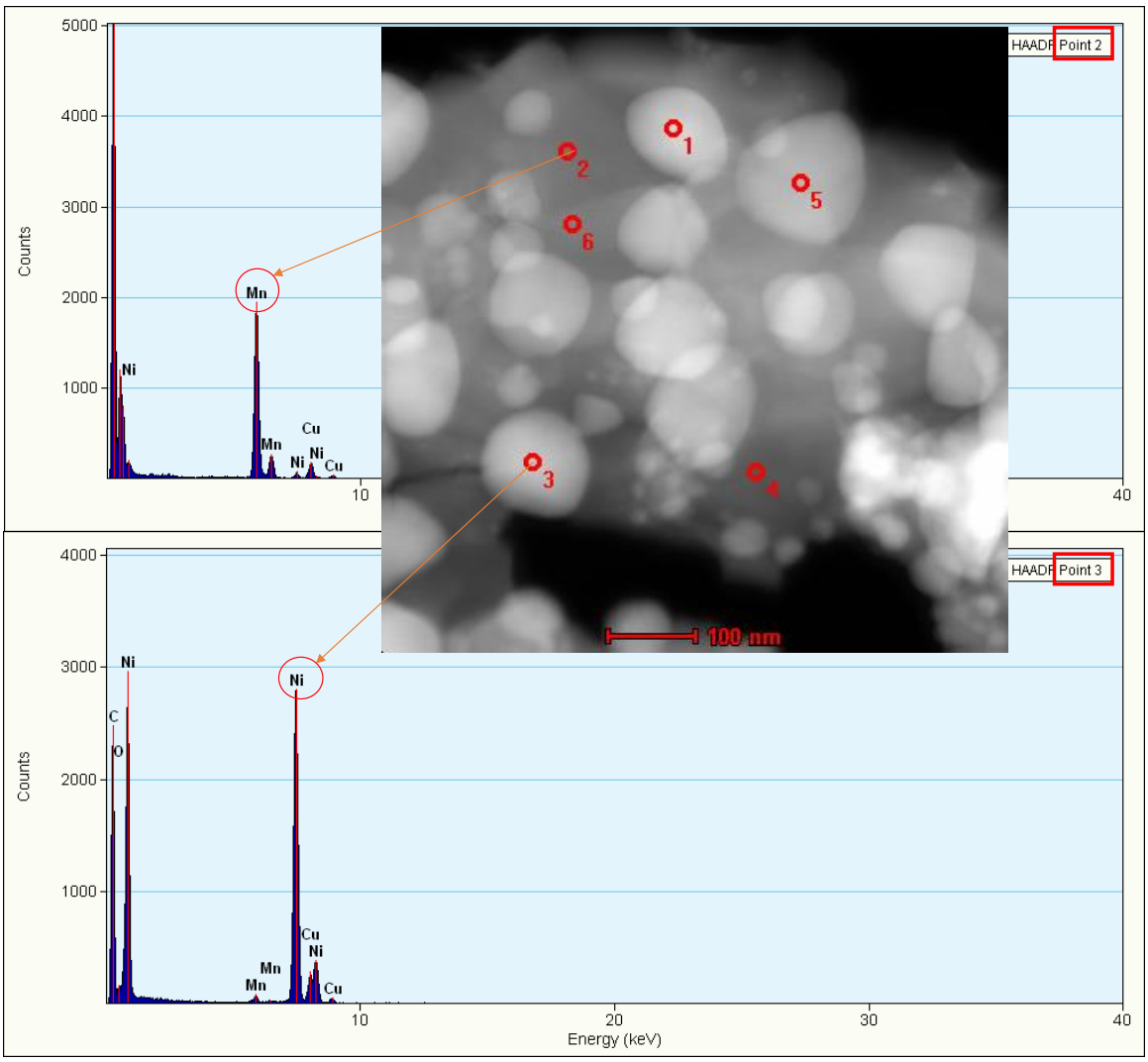

Figure S2. TEM elemental analyses results of $(MnO)_{0.5}/(Ni)_{0.5}$ anode material at two different points

Table S1. List of some MnO anodes for lithium-ion batteries

Anode material	Delithiation capacity (mAh/g)	Percentage capacity retention after 30 cycles	Reference
MnO	~500	~60%	[26]
MnO	600	25%	[29]
MnO/C	~650	~85%	[27]
MnO/C	740	90%	[31]
$(MnO)_{0.8}/(Ni)_{0.2}$	596	78%	[this work]

References

1. H.J. Qiu, J.Q. Wang, P. Liu, Y. Wang, M.W. Chen, *Corrosion Science*, 96 (2015) 196
2. X. Xu, K. Shen, M. Wen, Q. Wu, G. Hou, H. Cao, L. Wu, G. Zheng, Y. Tang, *Applied Surface Science*, 450 (2018) 356
3. M. Riegraf, A. Zekri, M. Knipper, R. Costa, G. Schiller, K.A. Friedrich, *J. Power Sources*, 380 (2018) 26
4. J. Zhao, X. Xu, W. Zhou, Z. Zhu, *Fuel Processing Technology*, 161 (2017) 241
5. S. Chen, Y. Li, B. Wu, Z. Wu, F. Li, J. Wu, P. Liu, H. Li, *Electrochimica Acta*, 275 (2018) 40
6. J Lin, H. Jia, H. Liang, S. Chen, Y. Cai, J. Qi, C. Qu, J. Cao, W. Fei, J. Feng, *Chemical Eng. Journal*, 336 (2018) 562
7. S. Vijayakumar, S. Nagamuthu, K.S. Ryu, *Electrochimica Acta*, 238 (2017) 99
8. P.L. Taberna, S. Mitra, P. Poizot, P. Simon, J.M. Tarascon, *Nature Materials*, 5 (2006) 567
9. Q. Liu, J. Huo, Z. Ma, Z. Wu, S. Wang, *Electrochimica Acta*, 206 (2016) 52
10. Y. Han, K. Yang, P. Jing, B. Xue, W. Ma, *J. Alloys Compounds*, 741 (2018) 765
11. Q. Wu, L. Li, Y.D. Zhang, W.J. Shui, *Composites B, Engineering*, 131 (2017) 1
12. C. Li, Y. Qi, X. Peng, X. Hao, D. Li, *J. Luminescence*, 169 (2016) 191
13. M. Usui, T. Satoh, H. Kimura, S. Tajima, Y. Hayashi, D. Setoyama, M. Kato, *Microelectronics Reliability*, 78 (2017) 93
14. L. Yin, M. Wu, Y. Li, G. Wu, Y. Wang, Y. Wang, *New Carbon Materials*, 32 (2017) 311
15. C. Hsieh, C. Lin, Y. Chen, J. Lin, *Electrochimica Acta*, 111 (2013) 359
16. D.S. Kim, G.H. Lee, S. Lee, J.C. Kim, H.J. Lee, B.K. Kim, D.W. Kim, *J. Alloys Compounds*, 707 (2017) 275
17. Y. Tang, H. Zhang, J. Li, G. Hou, H. Cao, L. Wu, G. Zheng, Q. Wu, *J. Alloys Compounds*, 719 (2017) 203
18. J. Yuan, X. Zhang, C. Chen, Y. Hao, R. Agrawal, C. Wang, W. Li, H. Yu, Y. Yu, X. Zhu, Z. Xiong, Y. Xie, Materials Letters, 190 (2017) 37
19. H. Liu, X. Wang, J. Wang, H. Xu, W. Yu, X. Dong, H. Zhang, L. Wang, *Scripta Materialia*, 139 (2017) 30
20. S. Liu, J. Xie, Y. Zheng, G. Cao, T. Zhu, X. Zhao, *Electrochimica Acta*, 66 (2012) 271
21. J. Yu, L. Zhu, C. Fan, C. Zan, L. Hu, S. Yang, Q. Zhang, W. Zhu, L. Shi, F. Wei, *Particuology*, 22 (2015) 89
22. J. Zang, J. Ye, H. Qian, Y. Lin, X. Zhang, M. Zheng, Q. Dong, *Electrochimica Acta*, 260 (2018) 783
23. M. Kunduraci, G.G. Amatucci, *J. Electrochemical Society*, 153 (2006) A1345
24. X. Kong, Y. Wang, J. Lin, S. Liang, A. Pan, G. Cao, *Electrochimica Acta*, 259 (2018) 419
25. Y. Ding, L. Chen, P. Pan, J. Du, Z. Fu, C. Qin, F. Wang, *Applied Surface Science*, 422 (2017) 1113
26. Y.J. Mai, D. Zhang, Y.Q. Qiao, C.D. Gu, X.L. Wang, J.P. Tu, *J. Power Sources*, 216 (2012) 201
27. S. Guo, G. Lu, S. Qiu, J. Liu, X. Wang, C. He, H. Wei, X. Yan, Z. Guo, *Nano Energy*, 9 (2014) 41
28. W. Luo, X. Hu, Y. Sun, Y. Huang, *ACS Appl. Mater. Interfaces*, 5 (2013) 1997
29. J. Zhang, W. Zhang, T. He, I.S. Amiinu, Z. Kou, J. Li, S. Mu, *Carbon*, 115 (2017) 95
30. X. Fan, S, Li, L. Lu, *Electrochimica Acta*, 200 (2016) 152
31. W. Zhu, H. Huang, W. Zhang, X. Tao, Y. Gan, Y. Xia, H. Yang, X. Guo, *Electrochimica Acta*, 152 (2015) 286